RSC Advances

PAPER

View Article Online
View Journal | View Issue

Cite this: *RSC Adv.*, 2022, **12**, 26908

The effect of *Bacillus cereus* LV-1 on the crystallization and polymorphs of calcium carbonate

Guoguo Yang, Fuchun Li, * Yazhi Wang, Chen Ji, Lingjie Huang, Zhimeng Su, Xuelin Li and Chonghong Zhang

The study of $CaCO_3$ polymorphism is of great significance for understanding the mechanism of carbonate mineralization induced by bacteria and the genesis of carbonate rock throughout geological history. To investigate the effect of bacteria and shear force on $CaCO_3$ precipitation and polymorphs, biomineralization experiments with *Bacillus cereus* strain LV-1 were conducted under the standing and shaking conditions. The results show that LV-1 induced the formation of calcite and vaterite under the standing and shaking conditions, respectively. However, the results of mineralization in the media and the $CaCl_2$ solution under both kinetic conditions suggest the shear force does not affect the polymorphs of calcium carbonate in abiotic systems. Further, mineralization experiments with bacterial cells and extracellular polymeric substances (EPS) were performed under the standing conditions. The results reveal that bacterial cells, bound EPS (BEPS), and soluble EPS (SEPS) are favorable to the formation of spherical, imperfect rhombohedral, and perfect rhombohedral minerals, respectively. The increase in the pH value and saturation index (SI) caused by LV-1 metabolism under the shear force played key roles in controlling vaterite precipitation, whereas bacterial cells and EPS do not play roles in promoting vaterite formation. Furthermore, we suggest that vaterite formed if pH > 8.5 and SI_{ACC} > 0.8, while calcite formed if pH was between 8.0–9.0 and SI_{ACC} < 0.8. Bacterial cells and BEPS are the main factors affecting $CaCO_3$ morphologies in the mineralization process of LV-1. This may provide a deeper insight into the regulation mechanism of the polymorphs and morphologies during bacterially induced carbonate mineralization.

Received 10th July 2022
Accepted 3rd September 2022

DOI: 10.1039/d2ra04254a

rsc.li/rsc-advances

Introduction

Microbial induced carbonate precipitation (MICP) is a common phenomenon in nature and plays a major role in the geochemical cycling of elements and cementation of natural systems.[1,2] The study of MICP is also important for exploring the potential of CO_2 sequestration, metal bioremediation, and restoration of historical stones and concrete.[3,4] Hence, many studies have been conducted to understand the MICP mechanism.[1,5,6] Microbes have been shown to enhance alkalinity and saturation index (SI) *via* metabolism, thus, inducing carbonate precipitation.[7] Bacterial cells and extracellular polymeric substances (EPS) can influence the nucleation and growth of minerals by serving as nucleation sites.[8,9]

Calcium carbonate ($CaCO_3$) has three anhydrous crystalline polymorphs, calcite, aragonite, and vaterite, as well as one amorphous calcium carbonate (ACC). Calcite is the most stable, and aragonite and vaterite are generally metastable minerals. Most studies have focused on the formation of $CaCO_3$ precipitation in abiotic systems and highlighted that pH and the concentrations of Ca^{2+} and dissolved inorganic carbon ions can control the formation of $CaCO_3$ precipitation.[10–13] In addition to the above variables, $CaCO_3$ precipitation is affected by nucleation sites in the process of MICP.[14] The shear force applied through a shaker can increase dissolved oxygen and directly affect these factors *via* accelerating microbial metabolic rates. The most common experiments use standing incubation to study the mechanism of MICP, while some research has accelerated carbonate precipitation by shaking incubation to achieve specific engineering goals.[15] Previous studies[5,16–21] have shown that calcium carbonate mineralized in the form of calcite with the participation of several bacteria under the standing condition, and precipitated in the form of unstable ACC and/or vaterite under the shaking condition (Table 1), the results between the standing and shaking conditions are different, in part, due to shear force. To the best of our knowledge, few research reports have reported the role of shear force on MICP. Guo *et al.*[22] compared calcium carbonate species induced by three bacterial strains under shaking and standing incubation, this showed that *Bacillus* sp. and *Lysinibacillus* sp. induced the formation of calcite, while *Microbacterium* sp. mediated the

College of Resources and Environmental Sciences, Nanjing Agricultural University, Nanjing, 210095, China. E-mail: fchli@njau.edu.cn

Table 1 List of relevant experimental conditions and results[a]

Kinetic condition	Species	Nutrient components	Incubation time (d)	Mineral	Ref.
Standing	*Bacillus cereus*	Tryptone, beef extract	20	C	This study
	Lysinibacillus sp.	Yeast extract, calcium acetate	18	C	Lü *et al.*[16]
	B. subtilis	Tryptone, yeast extract	24	C	Han *et al.*[5]
	S. pasteurii	Urea, peptone, beef extract, agar	1	C	Zhang *et al.*[17]
	B. mucilaginosus	Sucrose, yeast extract	3	C	Zheng and Qian[18]
	Bacillus cereus	Yeast extract, calcium acetate	40	C	Guo *et al.*[22]
	Lysinibacillus sp.	Yeast extract, calcium acetate	40	C	
	Microbacterium sp.	Yeast extract, calcium acetate	40	V	
Shaking	*Bacillus cereus*	Tryptone, beef extract	20	V	This study
	Lysinibacillus sp.	Yeast extract, calcium acetate	3	V	Lv *et al.*[19]
	B. subtilis	Tryptone, yeast extract	7	ACC, V	Liu *et al.*[20]
	S. pasteurii	Urea, peptone, beef extract	1	V	Zhang *et al.*[17]
	B. mucilaginosus	Sucrose, yeast extract	3	V, C	Zheng[21]
	Bacillus cereus	Yeast extract, calcium acetate	40	C	Guo *et al.*[22]
	Lysinibacillus sp.	Yeast extract, calcium acetate	40	C	
	Microbacterium sp.	Yeast extract, calcium acetate	40	V	

[a] C – calcite; V – vaterite.

formation of vaterite under two kinetic conditions. However, the authors in this report did not offer explanations for the effect of shear force on the MICP.

In this study, we explored the effect of bacteria and shear force on the mineralization of calcium carbonate, mineralization experiments of *Bacillus cereus* LV-1 were performed under the shaking and standing conditions. To further reveal the biomineralization mechanism of calcium carbonate, we also investigated the characteristics of calcium carbonate produced in the media and $CaCl_2$ solution under the shaking and standing conditions and the effect of different bacterial components (*i.e.*, native cells, BEPS, and SEPS) on the mineralization of $CaCO_3$. In addition, we discussed the effect of solution chemistry on the polymorphs of $CaCO_3$. The results of this study can provide scientific basis for understanding the role of shear force and bacteria in the formation of $CaCO_3$ precipitation, this is conducive to providing a reference for the application extension of MICP in engineering.

Materials and methods

Characterization of LV-1

A non-pathogenic LV-1 (*Bacillus cereus*) was bought from the China General Microbiological Culture Collection Center (CGMCC 1.15914).[9] A transmission electron microscope image shows that the cells are rod-shaped with a size of (1.0–1.2) μm × (4.0–6.0) μm (Fig. 1), arranged as a short or long chain. This is a spore-forming and Gram-positive (G^+) strain.

Bacterially mineralization experiments under the standing and shaking conditions

The liquid media (TB-C) used for the bacterial mineralization experiments consists of 5 g tryptone, 3 g beef extract, and 1.11 g calcium chloride ($CaCl_2$) in 1 L deionized water, under high-pressure steam sterilization (121 °C, 103.4 kPa, 20 min). The solid media was obtained by adding 2% agar powder to the liquid media, and used to purify bacteria. The initial pH value was adjusted to 7.5 using 0.5 mol l^{-1} sodium hydroxide (NaOH) solution, and dropped to 7.28 after sterilization.

To avoid the interference of calcium carbonate precipitation on experimental results, a single colony cultivated on the agar plate for 24 hours after purification was inoculated into the media without $CaCl_2$ (TB media) to prepare bacterial inoculum and then placed in a shaking incubator (180 rpm) at 30 °C for 24 hours. Then, a 10 ml of bacterial inoculum was inoculated into each of 150 ml Erlenmeyer flask containing 90 ml sterilized TB-C media, yielding 100 ml of final bacterial solution. These flasks were placed in the standing and shaking incubators (180 rpm) at 30 °C for 20 days. The control experiments with dead bacteria (bacterial inoculum were sterilized at 121 °C for 20 min) were also conducted, denoted as Shaking-CK and Standing-CK.

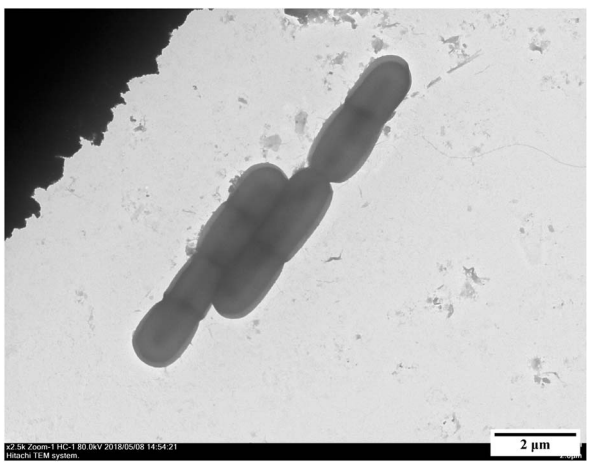

Fig. 1 Morphologies of bacterial cells (incubated on a solid medium after 24 h).[9]

Abiotic mineralization experiments under the standing and shaking conditions

To study further the role of shear force in the mineralization of calcium carbonate, mineralization experiments in the TB-C media and $CaCl_2$ solution were carried out in the system of gas diffusion. 25 ml of TB-C media and 10 mmol l^{-1} $CaCl_2$ solutions were added into a series of 50 ml flasks. Next, these flasks were placed in the two closed desiccators. A beaker with 5 g of $(NH_4)_2CO_3$ as the source of CO_2 was also placed in the desiccators. Next, a desiccator was placed in the standing incubator and another desiccator was placed in the shaking incubator (180 rpm) for 50 hours.

Separation of different bacterial components and their mineralization experiments

To study further the effect of different components in the bacterial solution on the mineralization of calcium carbonate, a series of mineralization experiments with bacterial cells, BEPS, and SEPS were conducted. The TB media containing LV-1 was centrifuged at 5000 rpm for 10 min to obtain the cells and supernatants (SN). The harvested cells were washed three times with 0.5% NaCl solution (w/v) to remove residual media and metabolic products and then resuspended for further use, denoted as bacterial cells. SN was filtered by using 0.22 μm cellulose acetate membranes and used to extract SEPS. SEPS in SN after filtration was precipitated by centrifugation (5000 rpm, 10 min) with ethanol overnight at 4 °C.[6]

The cation exchange resin (CER) was used to obtain BEPS.[23] The cells after washing were added to CER with a dosage of 30 g 100 ml^{-1}, followed by stirring for 12 hours at 4 °C. Then, the CER was removed by settlement for 5 min. The supernatants (SN1) were obtained by centrifugation at 5000 rpm for 10 min. SN1 was filtered using 0.22 μm cellulose acetate membranes, followed by ethanol addition with a volume ratio of 1 : 3. BEPS in SN1 after filtration was precipitated by centrifugation with ethanol overnight at 4 °C.[6] The bacterial cells, BEPS, and SEPS extracts were preserved in a freezer (~40 °C) before the mineralization experiments.

One milliliter of bacterial cells, SEPS, and BEPS were added into a series of 50 ml beakers containing 24 ml of $CaCl_2$ solution with a concentration of 10 mmol l^{-1}. Next, these beakers were also placed in the system of gas diffusion described above. The measurement results showed that BEPS and SEPS contain 556.20 and 113.04 mg g^{-1} polysaccharide, and 9.92 and 97.86 mg g^{-1} protein, respectively. The initial pH value was adjusted to 7.0 using 0.5 mol l^{-1} NaOH solution. In the control experiments (CK), 1 ml of deionized water was used instead of the bacterial component.

All of the above experiments were performed at 30 °C in triplicate, and all flasks and beakers were sealed using 0.22 μm polypropylene films. After sampling, the obtained samples were separated into solid and liquid fractions by centrifugation (5000 rpm, 10 min). The solid fractions were used to characterize minerals, and the liquid fractions were used for biochemical analyses.

Measurement of biochemical characterization

The plate counting method was used to measure bacterial density. The carbonic anhydrase (CA) activity, the content of extracellular polysaccharide and protein, was determined using an EnSight enzyme-labeling instrument (PerkinElmer, Singapore) *via p*-nitrophenol, sulfuric acid-anthrone, and Coomassie brilliant blue staining methods.

The pH value of every sample was measured with a pH meter (PHS-3BW, Bante Instruments, China). The Ca^{2+} concentrations were measured with an inductively coupled plasma optical emission spectrometer (Agilent 710, Agilent Technologies, USA). Furthermore, the carbonate and bicarbonate concentrations were analyzed using the double indicator neutralization titration method. SI with respect to the mineral is $\log\left(\frac{[Ca^{2+}] \times [CO_3{}^{2-}]}{K_{sp}}\right)$. $[Ca^{2+}]$ and $[CO_3{}^{2-}]$ are, respectively, the ion activity of Ca^{2+} and $CO_3{}^{2-}$. K_{sp} is the solubility product constant for the relevant mineral phase. K_{sp} values of ACC, vaterite, and calcite are $10^{-6.40}$, $10^{-7.91}$, and $10^{-8.48}$, respectively.[24,25]

Analysis and observation of mineral

Determination of mineral amount. The mineral particles were transferred to glass slides and dried in air. The mineral amount was determined by a digital analytical balance accurate to 0.1 mg.

Analysis of mineralogical composition. The mineralogical composition was analyzed using a Rigaku D/max-B (III) powder X-ray diffraction (XRD) with Cu-Kα radiation. The mineral sample was scanned continuously at 2° (2θ) min^{-1} from 10° to 60° (2θ) at 25 kV and 20 mA. The qualitative identification of mineral phases was performed using Jade 6.[26]

Observation of mineralogical morphology. A Carl Zeiss Supra55 field emission scanning electron microscopy (FE-SEM) with an Oxford Aztec X-Max 150 energy dispersive spectroscopy (EDS) was used to observe the mineral morphology. The mineral particles were mounted on aluminum stubs covered with copper-conductive adhesive tape and then coated with 8 nm platinum film before observation. The SEM observations were performed at an accelerating voltage of 5 kV.

Results

Biochemical characteristics under the shaking and standing conditions

In both kinetic conditions, LV-1 grew gradually, and bacterial density reached the logarithmic phase and then decreased sharply owing to the shortage of nutrients (Fig. 2a). The bacterial density reached its maximum on day 4 (2.63×10^7 cfu ml^{-1}) and day 2 (11.30×10^7 cfu ml^{-1}) for the standing and shaking bacterial experiments, respectively. The bacterial density was higher in the shaking than in the standing bacterial experiments because the shaking condition can provide more dissolved oxygen for bacterial growth and metabolism. Thus, the protein content and CA activity in the shaking bacterial experiments were also higher than those for the standing condition

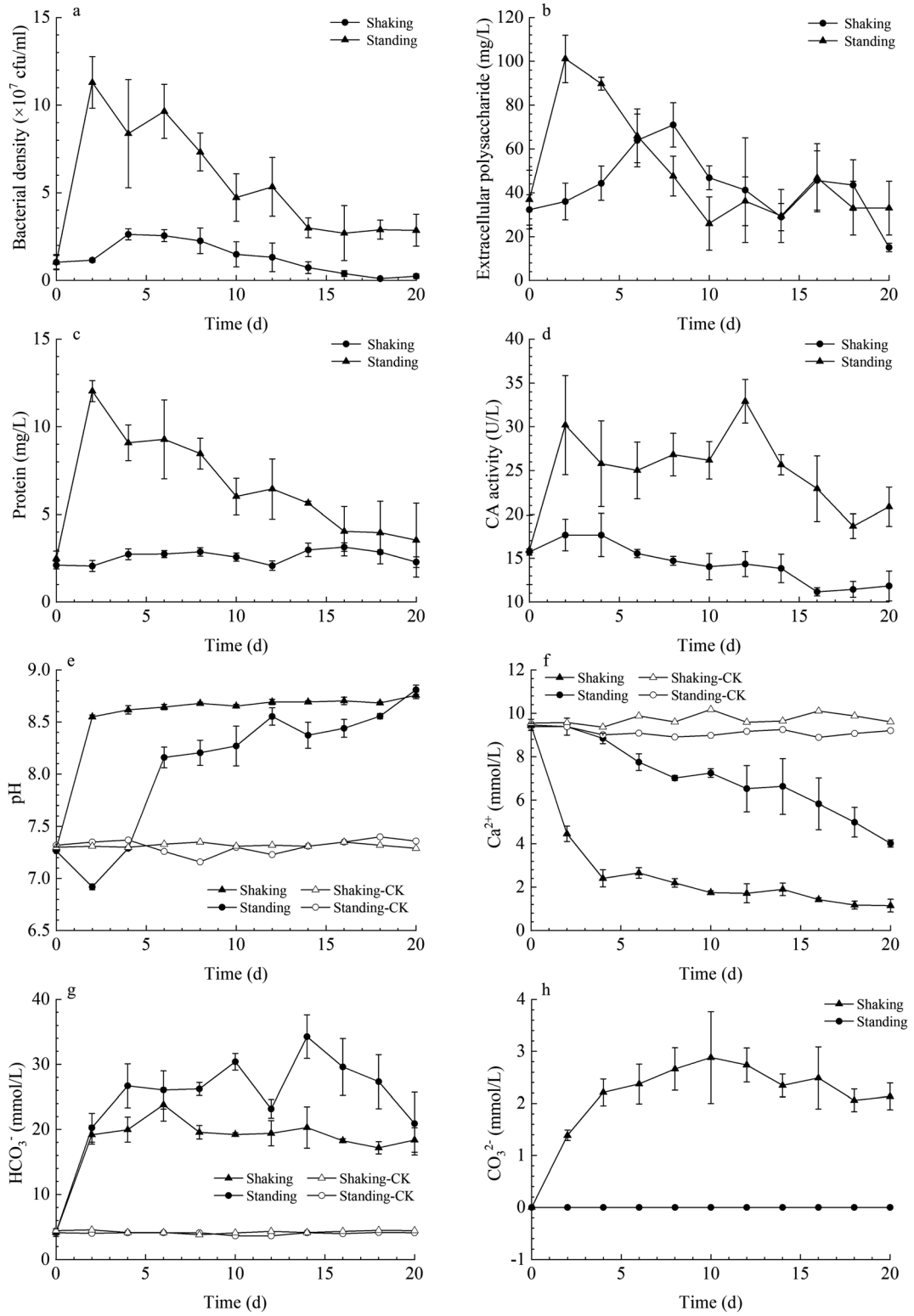

Fig. 2 Temporal changes of bacterial density (a), content of extracellular polysaccharide (b) and protein (c), CA activity (d), pH value (e), concentration of Ca^{2+} (f), HCO_3^- (g) and CO_3^{2-} (h) in the standing and shaking bacterial experiments.

(Fig. 2c and d). However, the content of extracellular polysaccharide in the shaking bacterial experiments was higher than that for the standing condition before day 6, while the content of extracellular polysaccharide in both the shaking and standing bacterial experiments was nearly the same on and after day 6 (Fig. 2b), we hypothesized the following: (1) bacterial

density decreased sharply after day 2 under the shaking condition, thus could secrete less polysaccharide; (2) higher bacterial density under the shaking condition easily caused the shortage of nutrients, thus the secreted polysaccharide in the early stages was depleted by LV-1 in the later stages by serving as a backup nutrient; (3) the secreted polysaccharide under the shaking condition was encapsulated in massive minerals by serving as nucleation template.

The pH value in both the shaking and standing bacterial experiments increased gradually until it remained nearly stable, while the pH value in the control groups remained stable from beginning to end. Prior to day 4, the pH in the shaking bacterial experiments increased faster than that in the standing bacterial experiments (Fig. 2e). The changes of HCO_3^- and CO_3^{2-} concentrations were monitored in both the shaking and standing bacterial experiments; Fig. 2g and h show that they increased gradually. However, the CO_3^{2-} concentrations were zero in the standing bacterial experiments (Fig. 2g and h). This is partly due to the concentration being lower than the detection limit in the standing bacterial experiments. Moreover, Ca^{2+} concentrations decreased gradually in both the shaking and standing bacterial experiments, though the decrease was faster in the shaking bacterial experiments than in the standing bacterial experiments (Fig. 2f), while it remained nearly stable in the control groups.

Mineral composition and morphologies in the standing and shaking experiments

The mineral amount in the standing bacterial experiments was initially zero, then gradually increased with time after day 6, reaching a maximum on day 20. The amount in the shaking bacterial experiments increased sharply at the beginning of the run and was always higher than that in the standing bacterial experiments (Fig. 3). However, no mineral precipitation took place in the CK experiments.

The XRD patterns of precipitates indicated that the mineral formed in the experiments with LV-1 under shaking condition from days 2 to 20 was only vaterite (Fig. 4a). However, the XRD patterns show that no visible diffraction peak was observed before day 12, and the diffraction peaks of calcite appeared between days 12 and 20 for the samples in the standing bacterial experiments (Fig. 4b).

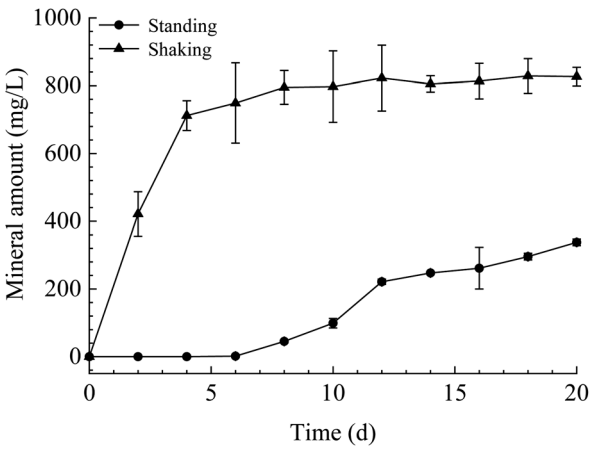

Fig. 3 Temporal changes of mineral amount in the shaking and standing bacterial experiments.

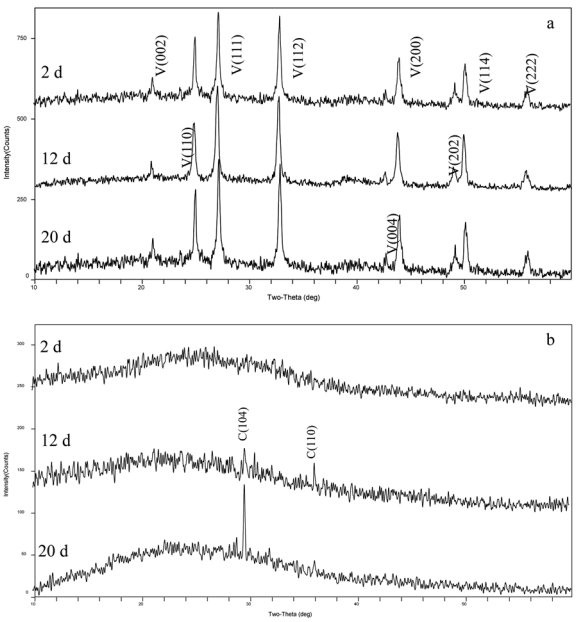

Fig. 4 XRD patterns of precipitates formed in the shaking (a) and standing (b) bacterial experiments. C – calcite; V – vaterite.

The FE-SEM images of mineral formed in the shaking bacterial experiments have countless spherical particles with a size of 10–40 μm. The pores encased within spherulites are chain-like, similar to bacterial cells (Fig. 5). The calcite formed in the standing bacterial experiments under FE-SEM displayed a variety of morphologies, including spherical, rod-shaped, and irregular particles with a size of 100–800 μm. The uniform-sized and rod-shaped particles show chain-like arrangements (Fig. 6). Moreover, the EDS spectrums from minerals formed in the standing and shaking bacterial experiments show signals from carbon (C), oxygen (O) (Fig. 5f and 6c), are calcium (Ca), suggesting that these minerals are calcium carbonate, in agreement with the XRD results (Fig. 4).

Abiotic mineralization experiments of calcium carbonate in the system by gas diffusion

To unveil the effect of shear force on the polymorphs and morphologies of calcium carbonate, mineralization experiments in the TB-C media and $CaCl_2$ solution were conducted by a gas diffusion method. In these experiments, $(NH_4)_2CO_3$ was decomposed to large amounts of NH_3 and CO_2, which caused the increase in pH and CO_3^{2-} in the solution. Then calcium carbonate can precipitate continuously when the supersaturation of calcium carbonate was reached. Our experimental results showed that the mineral amount in the shaking experiments was lower than that in the standing experiments (Fig. 7). The amount produced in the TB-C media was higher than that in the $CaCl_2$ solution.

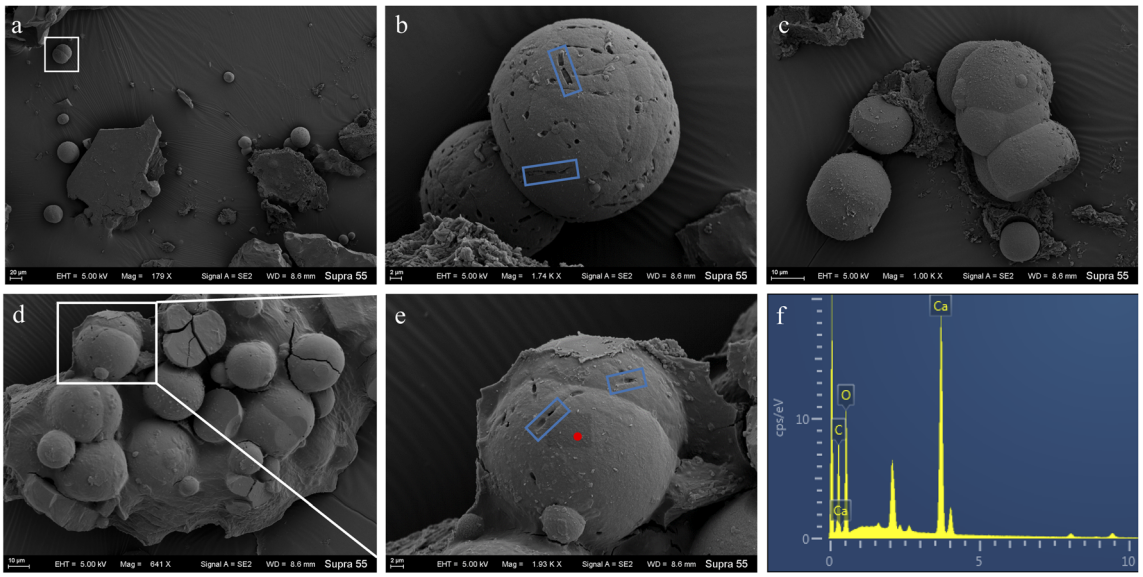

Fig. 5 FE-SEM images of carbonate mineral from the shaking bacterial experiments (a–c) spherulites and twin-spheres (marked with white rectangular boxes) on day 2, there are some pores as chain-like arrangement on the surface of spherulites (marked with blue rectangular boxes); (d) and (e) spherical and twin-spheres particles on day 20, the pores of chain-like arrangements encase within spherulites (marked with blue rectangular boxes); (f) EDS spectrum of the red dot in (e).

XRD analysis (Fig. 8) shows that there is only calcite in the precipitates of the two experiments of TB-C media, and the precipitated minerals are primarily calcite, with a little aragonite in $CaCl_2$ solution under the shaking and standing conditions. FE-SEM images (Fig. 9) show that flower-like, and spheroidal aggregates were obtained from the TB-C media under the shaking condition, the three structures are all stacked by the rhombohedral subunits. However, rhombohedra and flower-like stacked by the rhombohedral subunits were produced from TB-C media under the standing condition. FE-SEM images of the precipitated carbonate structures formed in the $CaCl_2$ solution under the shaking condition were dominated by rhombohedral morphologies. FE-SEM images of carbonate minerals precipitated from $CaCl_2$ solution under the standing condition were dominated by rhombohedral morphologies, with a minority of irregular particles stacked by needled-like subunits.

Mineralization of calcium carbonate in the system with different bacterial components

To unveil the effect of different components in the bacterial solution on the mineralization of calcium carbonate, a series of

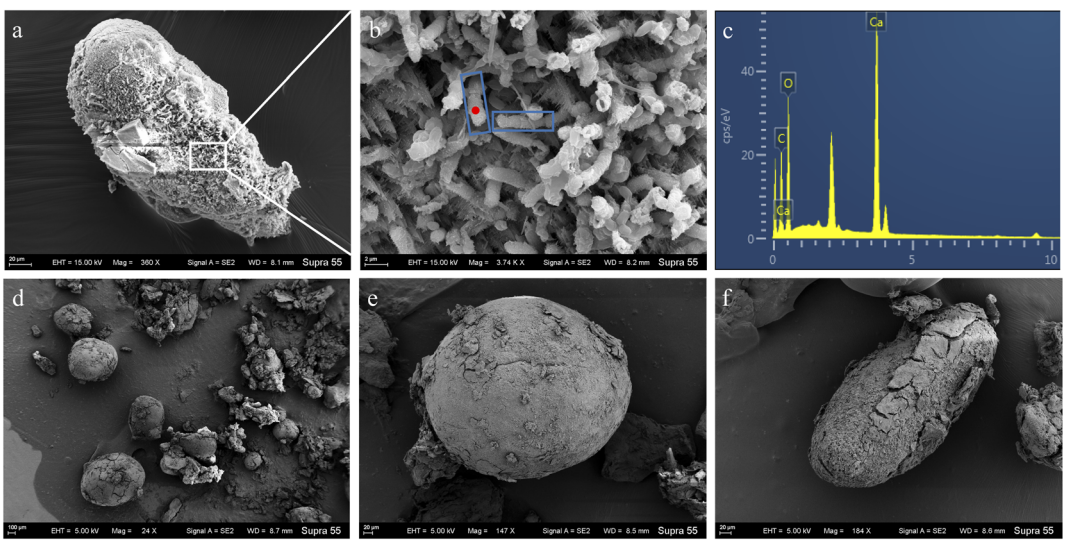

Fig. 6 FE-SEM images of carbonate mineral from the standing bacterial experiments. (a) and (b) Rod-shaped nanoparticles of macroscale crystal aggregates on day 12 show chain-like arrangements similar with bacterial cells (highlighted with blue rectangular boxes); (c) EDS spectrum of the red dot in (b); (d) spherulitic, rod-shaped, and irregular morphologies on day 20; (e) spherical mineral; (f) rod-shaped mineral.

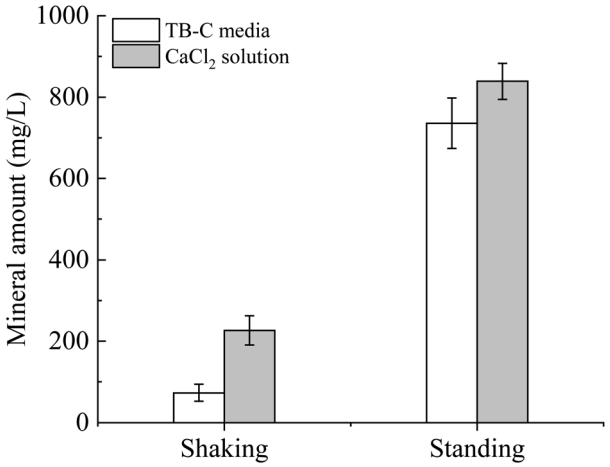

Fig. 7 Mineral amount in the system by gas diffusion under the shaking and standing conditions.

mineralization experiments with bacterial cells, BEPS, and SEPS were conducted in the system of gas diffusion. The results indicate that pH value, and HCO_3^- and CO_3^{2-} concentrations in the solution increased gradually with time owing to the decomposition of ammonium bicarbonate in the experiments with bacterial cells, BEPS, SEPS, and deionized water (Fig. 10a–c). Ca^{2+} concentrations drop gradually in these systems (Fig. 10d).

XRD analysis shows that the precipitated minerals are primarily calcite, with a little aragonite in the experiments with BEPS, SEPS, and deionized water (CK), while only diffraction peaks of calcite are observed in the batch of experiments with bacterial cells (Fig. 11 and Table 2). The FE-SEM images show that mineral morphologies were primarily imperfect rhombohedra with obtuse edges, with a little relatively perfect rhombohedra in the presence of BEPS, while plenty of perfect rhombohedra and little imperfect rhombohedra with obtuse edges were found in the experiments with SEPS (Fig. 12). FE-SEM images in the experiments with bacterial cells show that the morphologies of calcium carbonate are spherulite and irregular, with a few imperfect and perfect rhombohedra. CK groups were the same as the experiments of $CaCl_2$ solution under the standing condition, and thus only a sample was observed under FE-SEM. In addition, Table 2 shows that the crystal sizes obtained from bacterial cells, BEPS, and SEPS experiments are much smaller than those of the CK experiments.

Discussion

The effect of shear force on calcium carbonate crystallization

The experimental results showed that the precipitates amount in the shaking bacterial experiments was higher than that in the standing bacterial experiments. While the amount under the shaking condition was lower than that under the standing condition in abiotic experiments, this may be partly due to that the standing condition can create a diffusion-limited environment that allows local solution SI to increase to extreme levels, thus accelerating $CaCO_3$ precipitation. Therefore, it was suggested that the shear force significantly accelerated LV-1 metabolic activity by offering more dissolved oxygen, thus promoting $CaCO_3$ precipitation. Firstly, LV-1 can secrete more extracellular CA under shear force (Fig. 2d), which significantly accelerated CO_2 hydration processes and produced more HCO_3^- in solution,[27] we observed a higher HCO_3^- concentration under the shaking condition than that under the standing condition (Fig. 2g). Secondly, LV-1 metabolic activity can increase pH values,[9] the pH in the shaking bacterial experiments was higher than that in the standing bacterial experiments (Fig. 2e), thus

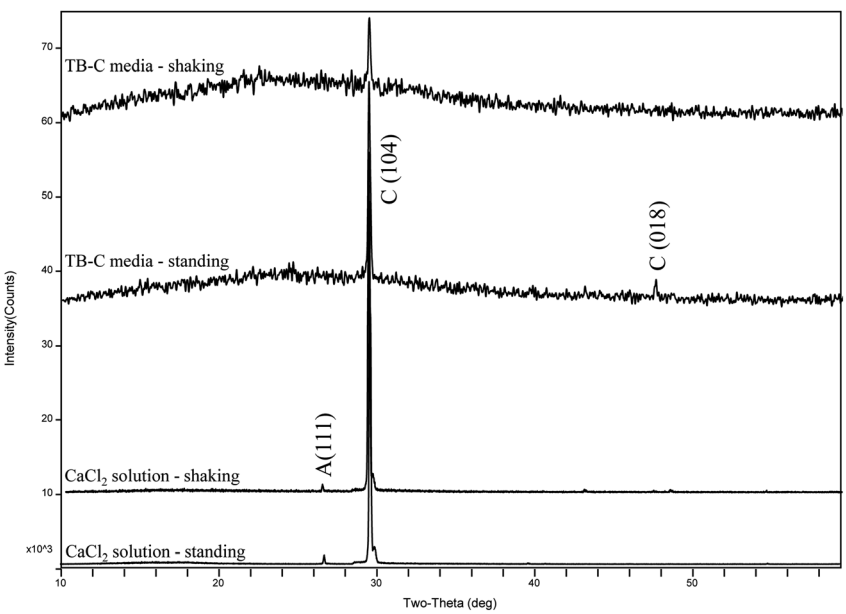

Fig. 8 XRD patterns of precipitates formed in the system by gas diffusion under the shaking and standing conditions.

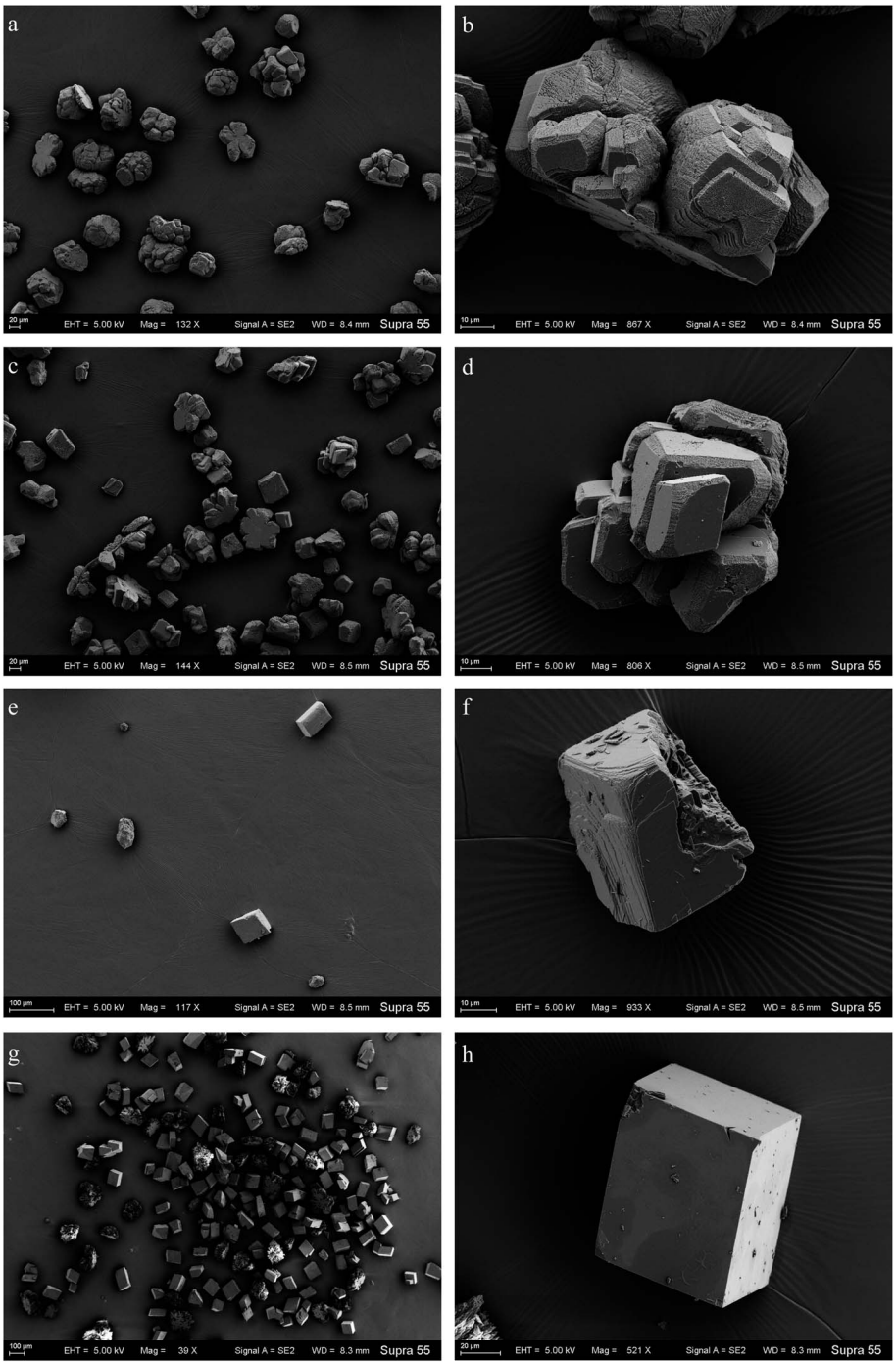

Fig. 9 FE-SEM images of the products mineralized in the TB-C media under the shaking (a, b) and standing (c, d) conditions; $CaCl_2$ solution under the shaking (e, f) and standing (g, h) conditions.

promoted more $CaCO_3$ precipitation. Thirdly, the results of bacterial experiments showed that bacterial cells, polysaccharide, and protein under the shaking condition were more abundant than under the standing condition (Fig. 2a–c), thus could induce more mineral crystallization. (i) Ca^{2+} concentrations in bacterial cells and EPS experiments were reduced more than in their CK experiments (Fig. 10d). (ii) Based on classical theory,[28] bacterial cells and EPS nucleation are more likely to occur.

The experimental results show that there is only calcite in the precipitates of the standing bacterial experiments, and only vaterite in that of the shaking bacterial experiments (Fig. 4), this is consistent with the results of many studies.[5,16–21] However, there are also inconsistent results in previous studies. For example, Guo *et al.*[22] suggested that shear force does not affect the polymorphs of calcium carbonate. To the best of our knowledge, this is the only study on the effect of shear force on bacterially induced calcium carbonate. Mineral collection

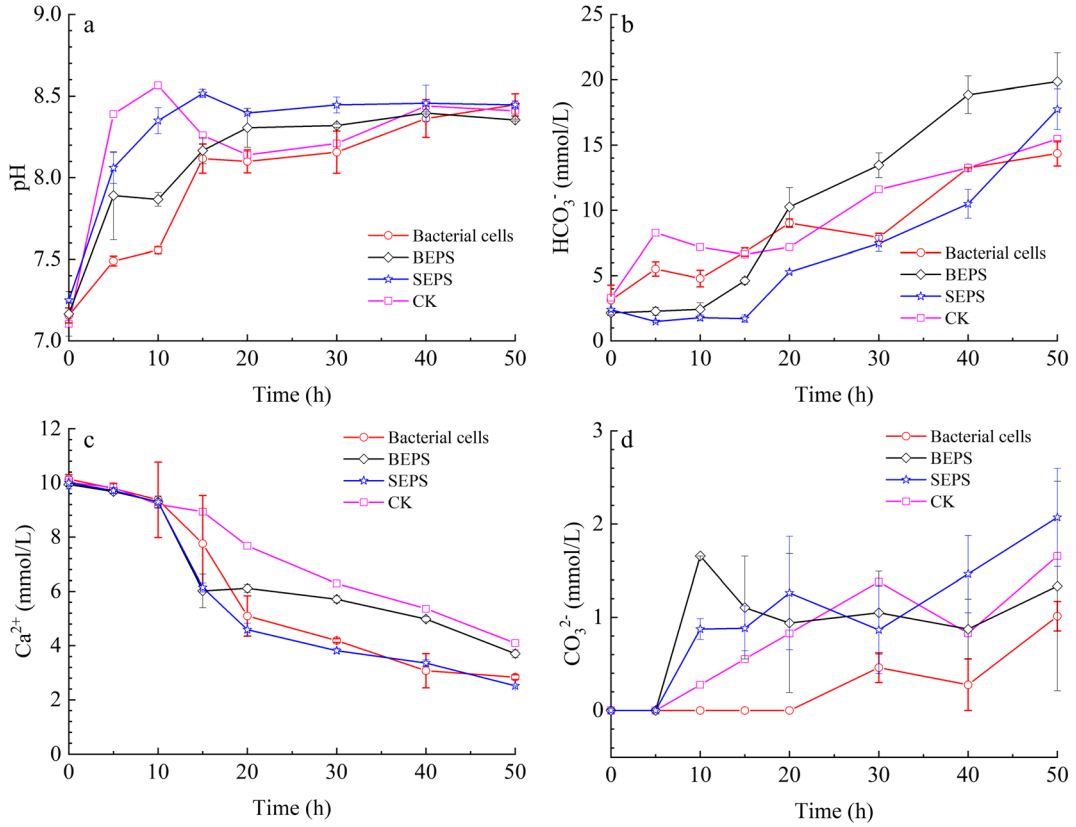

Fig. 10 Temporal changes of pH value (a), concentration of HCO_3^- (b), CO_3^{2-} (c), and Ca^{2+} (d) in the mineralization experiments with bacterial cells, BEPS, SEPS, and deionized water (CK).

occurred on day 40 in the study by Guo *et al.*,[22] which is significantly longer than other studies (<24 d, see Table 1). Vaterite induced by bacteria was reported to transform into calcite when the incubation time was prolonged.[17,29] We speculate the results shown by Guo *et al.*[22] may be partly due to the transformation of unstable phases for *Bacillus cereus* and *Lysinibacillus* sp., whereas *Microbacterium* sp. may control vaterite formation and stability; thus, vaterite formed under both kinetic conditions. Based on the above analysis, we suggest that shear force has a significant effect on the polymorphs of calcium carbonate in the bacterial system. The precipitated minerals under both kinetic conditions are both calcite in the

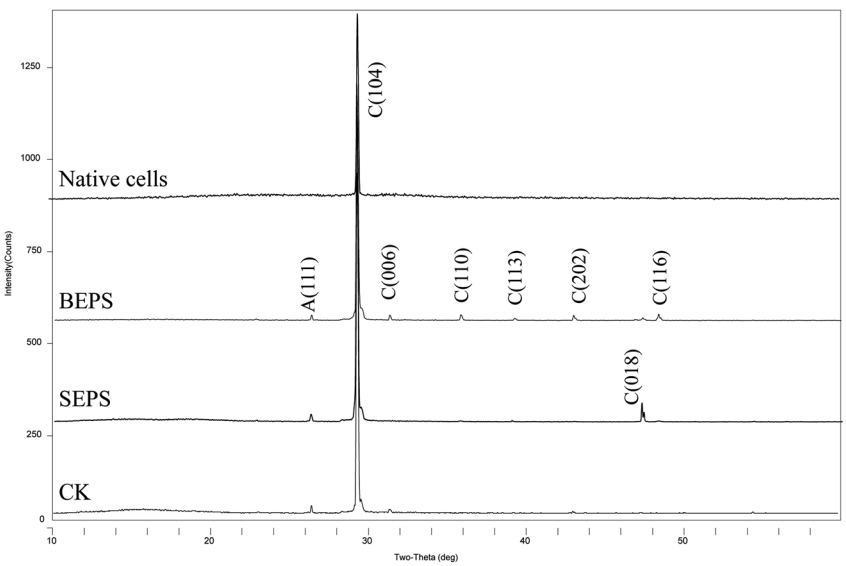

Fig. 11 XRD patterns of precipitates formed in mineralization experiments of different bacterial components. C – calcite; A – aragonite.

Table 2 The properties of minerals precipitated in the experiments with different bacterial components[a]

Batch	Mineral (mol%)	Main morphologies	Particle size (μm)
Bacterial cells	C	30% spherulite, 35% imperfect rhombohedra, 13% perfect rhombohedra, 22% irregular	10–300
BEPS	C (89) + A (11)	40% imperfect rhombohedra, 59% perfect rhombohedra	10–200
SEPS	C (92) + A (8)	79% perfect rhombohedra, 21% imperfect rhombohedra	5–150
CK (Fig. 9g and h)	C (90) + A (10)	77% rhombohedra and 23% irregular	100–300

[a] C – calcite; A – aragonite. The proportion of main morphologies was determined by imageJ based on SEM images.

TB-C media, and primarily calcite, with a little aragonite in the $CaCl_2$ solution, suggesting shear force has no effect on the polymorphs of calcium carbonate in abiotic systems. Therefore, discrepancies between the results of standing and shaking conditions are primarily caused by the solution chemistry and bacterial organic components. In the next section, we discuss the effect of different factor(s) on the $CaCO_3$ polymorphs.

The role of solution chemistry on calcium carbonate polymorph selection

The results of bacterial experiments show that shear force caused a dramatic rise in the solution chemistry, and thus, induced the formation of vaterite. The shaking bacterial experiments caused a greater increase in pH than the standing bacterial experiments (Fig. 2e). The phases precipitated are different in different pH ranges; calcite forms at low pH (9.0–9.5), and the crystallization of vaterite occurs at high pH (9.75–10.0).[30] In addition, a neutral pH was shown to drive calcite crystallization, while a higher pH (~11.5) promoted the formation of vaterite.[31] Moreover, pH was respectively in the range of 8.5–9.0 and lower than 8.5 for the crystallization of vaterite[19,20] and calcite[16] in the biotic experiments. Therefore, the effect of pH value on the polymorphs of calcium carbonate is potentially related to the ratio of CO_3^{2-}/HCO_3^-, which may

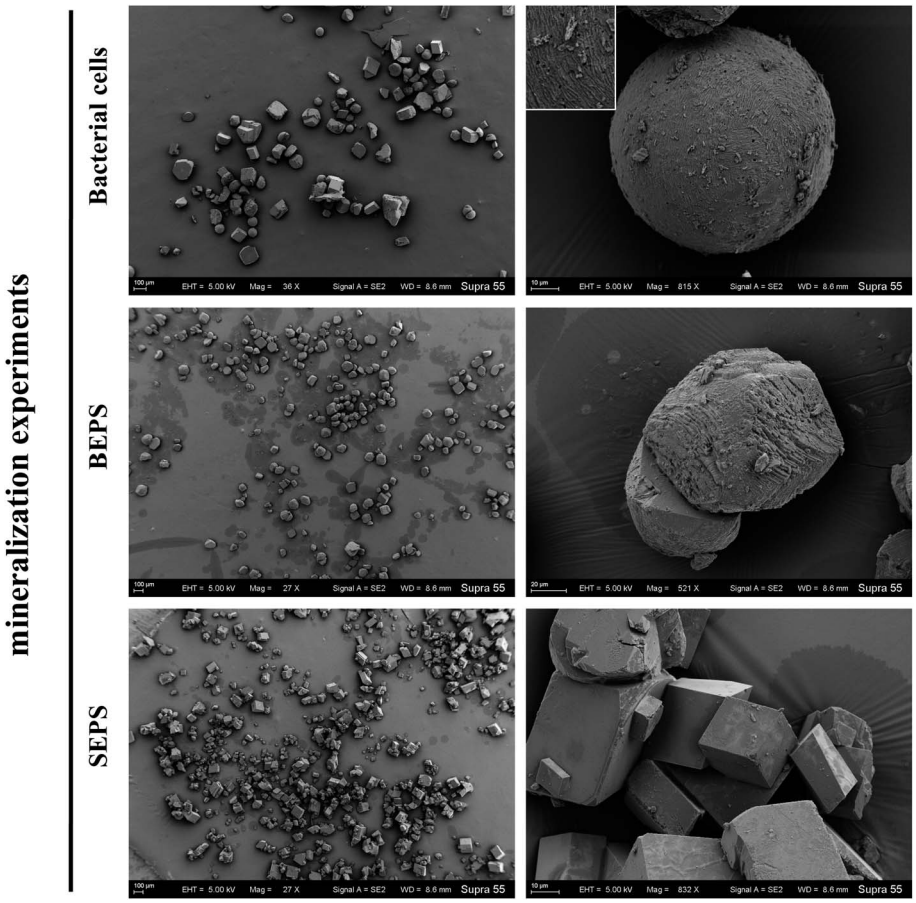

Fig. 12 FE-SEM images and EDS spectrum of precipitates formed at 50th hours in the experiments with different bacterial components. Bacterial cells: spherulite (marked with white circles), imperfect rhombohedra with obtuse edges (marked with white arrows), perfect rhombohedra and irregular. BEPS: imperfect rhombohedra with obtuse edges and perfect rhombohedra; SEPS: perfect rhombohedra and rhombohedra with obtuse edges.

affect the structure of prenucleation clusters to crystalline polymorphs.[11] In the CO_2–H_2O system, HCO_3^- species dominate when the pH value is below 8.35, and the proportion of CO_3^{2-} species increases when the pH value is above 8.35 (ref. 32). In this study, the CA secreted by LV-1 catalyzed the hydration of CO_2, which can provide CO_3^{2-} and HCO_3^- for the solution. The results of the shaking bacterial experiments depict a CO_3^{2-}/HCO_3^- ratio of 0.07–0.14, while it is close to zero in the standing bacterial experiments, *i.e.*, HCO_3^- becomes the sole species (Fig. 2g and h). A high CO_3^{2-}/HCO_3^- ratio is beneficial to the formation of less stable minerals.[11] Thus, the pH value is a possible influential factor *via* controlling the CO_3^{2-}/HCO_3^- ratio.

As mentioned above, calcite and vaterite formed under the standing and shaking conditions, respectively. The calculated results show that SI values in the shaking bacterial experiments were greater than those in the standing bacterial experiments, and SI values with respect to minerals gradually decrease through calcite, vaterite, and ACC (Fig. 13). Only calcite occurred in the precipitates in the experiments with bacterial cells, in which the SI_{ACC} value was lower than that in other experiments by gas diffusion (*i.e.*, BEPS, SEPS, and CK) (Fig. 14). These results indicate that a higher SI_{ACC} value is beneficial to the formation of unstable mineral phases, such as vaterite and aragonite. *M. xanthus* experiments also showed that high supersaturation was an important physicochemical factor for the formation of vaterite.[24] Ahn *et al.*[13] used experimental data to suggest that the supersaturation level for the precipitation of vaterite was higher than those of calcite precipitation. It was found that crystallization of calcium carbonate occurs *via* stable prenucleation clusters to different ACC forms, which eventually transform into particular crystalline polymorphs.[12] The results show that SI_{ACC} was less than 0.8, and calcite formed in the standing bacterial experiments and those with bacterial cells (Fig. 13 and 14). Although the SI value is supersaturated with respect to vaterite and aragonite, it is possible that an amorphous precursor of vaterite and aragonite requires a higher SI value. Therefore, a higher SI_{ACC} value is a key factor controlling the formation of vaterite and aragonite, and low SI_{ACC} promoted calcite precipitation.

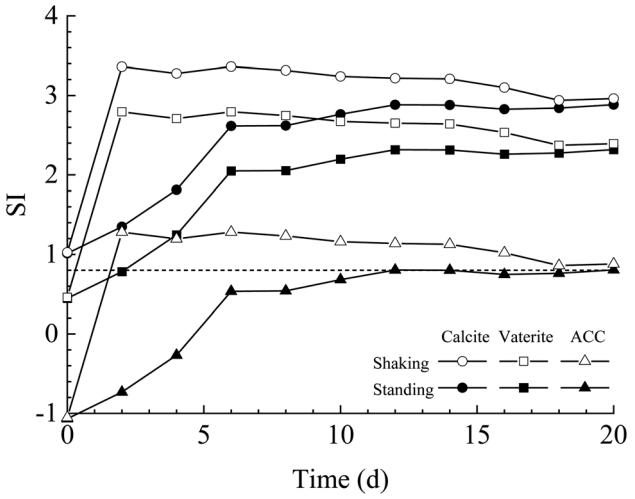

Fig. 13 Temporal changes of SI value in the solution under the shaking and standing conditions.

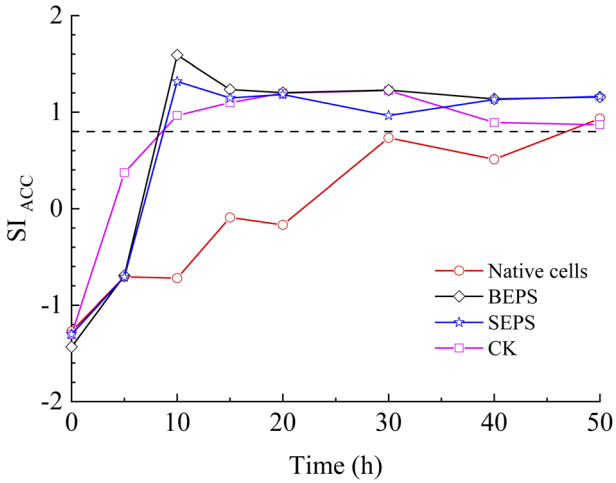

Fig. 14 Temporal changes of SI_{ACC} in the experiments with bacterial cells, BEPS and SEPS.

Based on bacterial experiments and those from gas diffusion, we simulated the stability field of vaterite, calcite, and aragonite. SI of different $CaCO_3$ forms is not the same. Based on a thermodynamic view of nucleation and growth, ACC is the precursor of anhydrous crystalline polymorphs.[33] In this paper, the stability field of vaterite, calcite, and aragonite was evaluated by SI_{ACC} value. The results show that vaterite formed at pH higher than 8.5 and SI_{ACC} higher than 0.8; calcite precipitated at pH 8.0–9.0 and SI_{ACC} lower than 0.8, while pH lower than 8.5 and higher SI_{ACC} higher than 0.8 drove the crystallization of calcite and aragonite (Fig. 15).

Effect of bacterial components on the polymorphs and morphologies of calcium carbonate

According to the results of two kinetic bacterial experiments, shear force changes the amount of polysaccharide and protein except for solution chemistry. To unveil the effect of BEPS and SEPS in the bacterial solution on the polymorphs and morphologies of calcium carbonate, bacterial cells, BEPS, and SEPS were separated from the bacterial solution, and their mineralization experiments were performed by the gas diffusion method. In these experiments, the precipitates formed in the experiments with BEPS and SEPS, as well as in CK groups were primarily calcite and a small amount of aragonite (Fig. 11 and Table 2). However, bacterial cells induced calcite precipitation. According to Fig. 10, pH and concentrations of CO_3^{2-} and HCO_3^- in the solution with bacterial cells are lower than BEPS, SEPS, and CK. Bacterial cells used in the mineralization experiments with gas diffusion were active and may secrete low-molecular-mass organic acids, leading to the slight lowering of pH.[6] In addition, the organic components of bacterial cells may chelate Ca^{2+} ions in solution.[23] These two processes reduce the supersaturation of carbonate, favoring calcite precipitation over aragonite. These results further demonstrated that $CaCO_3$

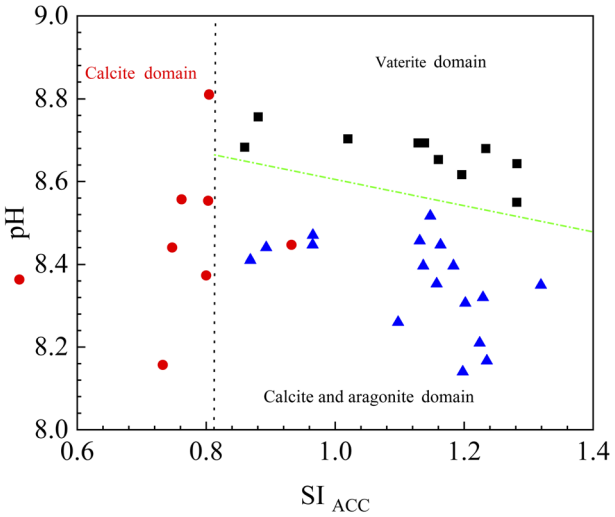

Fig. 15 The sketch of stability field for vaterite, calcite and aragonite. The data are from this paper.

polymorphs are controlled by solution chemistry. Nevertheless, our observation is consistent with other studies. For example, Ercole *et al.*[34] isolated EPS from *Bacillus firmus* and *Nocardia calcarea*, and only calcite crystallized in the presence of EPS. Yin *et al.*[35] also reported that EPS of *P. putida* induce calcite precipitation. Moreover, Tourney and Ngwenya[23] found that EPS produced by *Bacillus licheniformis* can inhibit vaterite precipitation, and proposed that dissolved organic carbon released from EPS complexes Ca^{2+} ions in the solution, reducing calcium carbonate saturation and favoring calcite precipitation over vaterite. Kawaguchi and Decho[36] suggested that biochemical composition of EPS influences $CaCO_3$ polymorph selection, polysaccharide was favorable to precipitation of calcite. According to the biochemical composition of BEPS and SEPS, polysaccharide content was all higher, thus more calcite precipitated. The results show the precipitates formed in the experiments with BEPS and SEPS were primarily calcite (~90%) (Table 2), while their CK groups formed 90% calcite and 10% aragonite. This suggests that BEPS and SEPS do not disturb $CaCO_3$ polymorphs selection in this paper. Therefore, bacterial cells and EPS of LV-1 exert less role on vaterite formation.

The results indicated that BEPS produced more imperfect rhombohedral minerals, and SEPS produced more perfect rhombohedral minerals. We speculate this occurred for one of two reasons: (1) the crystal morphologies formed in the presence of polysaccharides are more diverse than proteins.[37] Based on the biochemical composition of BEPS and SEPS, polysaccharide content in BEPS was higher than that in SEPS. (2) EPS can inhibit the relative growth rate of certain crystal faces through selective adsorption, affecting the crystal morphology and polymorphs. Based on the Bravais rule, crystal planes with fast growth rates tend to disappear, while those with slow growth rates remain on crystal.[38] Therefore, BEPS slow the growth rate of the (110), (116), and (202) crystal planes in this study, while SEPS inhibit the growth rate of the (018) crystal plane; thus, the mineral morphology induced by BEPS has a more complex structure than that in SEPS. Therefore, BEPS are beneficial to the formation of imperfect rhombohedra with obtuse edges.

A small number of $CaCO_3$ was reportedly nucleated onto cell walls for bacteria lacking BEPS, while a relatively large number of $CaCO_3$ was nucleated onto BEPS, and BEPS were encrusted by calcite crystals for bacteria containing BEPS.[39] Carbonate minerals first aggregate and grow at polar ends of bacterial cells, leading to the formation of dumbbell-shaped minerals, and then continue to grow into spherulite when bacteria exist in solution.[40,41] In the experiments with bacterial cells, morphologies of calcium carbonate are spherulite, irregular, imperfect rhombohedra, and perfect rhombohedra. The number of imperfect rhombohedra minerals is greater than that of perfect rhombohedra (Table 2). The EPS layer on bacterial cell surfaces may affect mineral nucleation and crystal growth, inducing the formation of imperfect rhombohedra minerals. In addition, spherical calcium carbonate is closely related to bacterial cells. In both the standing and shaking bacterial experiments, the morphology of calcium carbonate induced by LV-1 is primarily spherulite, the rod-like mineral particles and hole on the mineral surface similar in shape and size to the bacterial cells (Fig. 5 and 6), which indicate that they are calcified bacteria developed by nucleation on the cell surface.[9] Therefore, bacterial cells and BEPS on the cell surface may act as main forms of nucleation sites and influence morphologies of calcium carbonate in the experiments with LV-1.

The effect of LV-1 on the crystallization of calcium carbonate

Based on the above results, the mechanism of calcium carbonate crystallization induced by LV-1 was speculated (Fig. 16). (1) The changes in pH and SI caused by the metabolic activity of LV-1 played a main role in the selection of the $CaCO_3$ polymorphs. The shear force had a direct influence on bacterial metabolic activity and caused dramatic increases in pH and SI (Fig. 2). When pH > 8.5 and SI_{ACC} > 0.8, vaterite formed, and when pH (8.0–9.0) and SI_{ACC} < 0.8, calcite crystallized. (2) Bacterial cells and EPS of LV-1 played a smaller role in the vaterite formation. (3) Many different morphologies were observed in the experiments with bacterial cells, BEPS, and SEPS, respectively (Fig. 12 and Table 2), suggesting that several bacterial components can act as sites of heterogeneous nucleation, and thus, cause crystal size decreases and change in mineral morphology. Bacterial cells, BEPS, and SEPS preferentially lead to the crystallization of spherical, imperfect rhombohedral, and perfect rhombohedral minerals, respectively. Therefore, spherical minerals in both the standing and shaking bacterial experiments can be considered closely related to bacterial cells (Fig. 5 and 6). (4) The experimental results suggest that shear force has no effect on the size of minerals in abiotic systems. We speculate that the following two aspects may be the main reasons that the crystal size in the standing bacterial experiments was bigger than that in the shaking bacterial experiments. (i) Compared with the standing condition, the organic matters (including bacterial cells, polysaccharide and protein) under the shaking condition were more

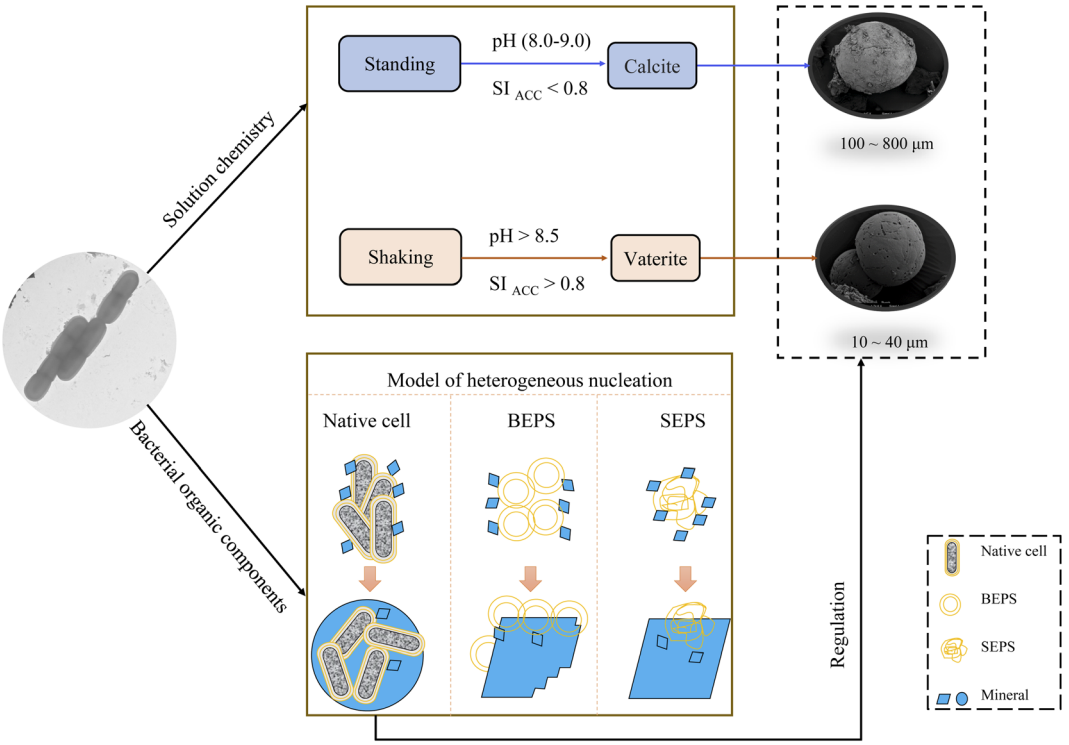

Fig. 16 The possible mechanism of calcium carbonate crystallization induced by LV-1.

abundant (Fig. 2) and provided more nucleation sites. (ii) The data on mineral amount and Ca^{2+} concentrations proved that the nucleation rate in the shaking bacterial experiments was faster than that in the standing bacterial experiments (Fig. 2f and 3). According to the classical theory of nucleation,[28] more nucleation sites and high nucleation rates can reduce the crystal size.

Conclusion

Two kinetic experiments (standing and shaking) with LV-1 and experiments with different bacterial components was conducted to investigate the role of LV-1 on the crystallization of calcium carbonate. (1) The bacterial mineralization experiments show that vaterite with a particle size of 10–40 μm precipitated in the shaking bacterial experiments, while calcite with a particle size of 100–800 μm formed in the standing bacterial experiments. However, the precipitated minerals were both calcite in the TB-C media, and calcite and aragonite in the $CaCl_2$ solution under shaking and standing conditions. This suggests that shear force has a great effect on the polymorphs and morphologies of calcium carbonate by affecting bacterial metabolism. (2) The mineralization experiments showed that the precipitates formed in the experiments with BEPS and SEPS, and CK groups were primarily calcite and aragonite; bacterial cells induced calcite precipitation. Bacterial cells, BEPS, and SEPS respectively induced the formation of spherical, imperfect rhombohedral, and perfect rhombohedral minerals, and reduced the crystal size of the calcium carbonate. Bacterial cells and BEPS are the main factors affecting morphologies of calcium carbonate in the experiments with LV-1 and have less influence on the vaterite formation.

Author contributions

Guoguo Yang: conceptualization, methodology, software, data curation, writing – original draft, and writing – review & editing. Fuchun Li: supervision, funding acquisition, writing – review & editing. Yazhi Wang & Chen Ji: investigation, data curation. Lingjie Huang: methodology, visualization, Zhimeng Su: software. Xuelin Li: validation. Chonghong Zhang: funding acquisition.

Conflicts of interest

The authors report no declarations of interest.

Acknowledgements

This work was supported by the Second Tibetan Plateau Scientific Expedition and Research [grant no: STEP 2019QZKK0707], the National Natural Science Foundation of China [grant no: 41673083 and 42273080], and the Natural Science Foundation of Jiangsu Province [grant no: BK20200564].

Notes and references

1 H. Li, Q. Z. Yao, F. P. Wang, Y. R. Huang, S. Q. Fu and G. T. Zhou, *Geochim. Cosmochim. Acta*, 2019, **256**, 35–48.
2 T. Zhu and M. Dittrich, *Front. Bioeng. Biotechnol.*, 2016, **4**, 4.

3 N. K. Dhami, M. S. Reddy and A. Mukherjee, *Front. Microbiol.*, 2013, **4**, 314.
4 W. Qin, C. Y. Wang, Y. X. Ma, M. J. Shen, J. Li, K. Jiao, F. R. Tay and L. N. Niu, *Adv. Mater.*, 2020, **32**, e1907833.
5 Z. Han, J. Wang, H. Zhao, M. E. Tucker, Y. Zhao, G. Wu, J. Zhou, J. Yin, H. Zhang, X. Zhang and H. Yan, *Minerals*, 2019, **9**, 218.
6 G. Yang, L. Li, F. Li, C. Zhang and J. Lyu, *Micron*, 2021, **140**, 102980.
7 S. Saneiyan, D. Ntarlagiannis, J. Ohan, J. Lee, F. Colwell and S. Burns, *Ecol. Eng.*, 2019, **127**, 36–47.
8 Z. A. Al Disi, N. Zouari, M. Dittrich, S. Jaoua, H. A. S. Al-Kuwari and T. R. R. Bontognali, *Mar. Chem.*, 2019, **216**, 103693.
9 J. Lyu, F. Li, C. Zhang, L. Gower, S. Wasman, J. Sun, G. Yang, J. Chen, L. Gu, X. Tang and G. Scheiffele, *Chem. Geol.*, 2021, **559**, 119974.
10 C. R. Blue, A. Giuffre, S. Mergelsberg, N. Han, J. J. De Yoreo and P. M. Dove, *Geochim. Cosmochim. Acta*, 2017, **196**, 179–196.
11 Y. B. Hu, M. Wolthers, D. A. Wolf-Gladrow and G. Nehrke, *Crystal Growth & Design*, 2015, **15**, 1596–1601.
12 D. Gebauer, P. N. Gunawidjaja, J. Y. Peter Ko, Z. Bacsik, B. Aziz, L. Liu, Y. Hu, L. Bergström, C. W. Tai, T. K. Sham, M. Edén and N. Hedin, *Angew. Chem., Int. Ed.*, 2010, **49**, 8889–8891.
13 J. W. Ahn, J. H. Kim, H. S. Park, J. A. Kim, C. Han and H. Kim, *Korean J. Chem. Eng.*, 2005, **22**, 852–856.
14 F. Hammes and W. Verstraete, *Rev. Environ. Sci. Bio/Technol.*, 2002, **1**, 3–7.
15 T. Huang, L. Liu and S. Zhang, *Desalin. Water Treat.*, 2021, **215**, 147–159.
16 X. Lü, Q. He, Z. Wang, M. Cao, J. Zhao, J. Jiang, R. Zhao and H. Zhang, *Chem. Geol.*, 2019, **530**, 119331.
17 W. Zhang, Y. Ju, Y. Zong, H. Qi and K. Zhao, *Environ. Sci. Technol.*, 2018, **52**, 9266–9276.
18 T. Zheng and C. Qian, *Process Biochem.*, 2020, **91**, 271–281.
19 J. J. Lv, F. Ma, F. C. Li, C. H. Zhang and J. N. Chen, *J. Struct. Biol.*, 2017, **200**, 97–105.
20 R. Liu, S. Huang, X. Zhang, Y. Song, G. He, Z. Wang and B. Lian, *RSC Adv.*, 2021, **11**, 14415–14425.
21 T. Zheng, *J. Cryst. Growth*, 2021, **563**, 126096.
22 W. Guo, F. Li and C. Zhang, *Geol. J. China Univ.*, 2018, **24**, 33–40.
23 J. Tourney and B. T. Ngwenya, *Chem. Geol.*, 2009, **262**, 138–146.
24 C. Rodriguez-Navarro, C. Jimenez-Lopez, A. Rodriguez-Navarro, M. T. Gonzalez-Muñoz and M. Rodriguez-Gallego, *Geochim. Cosmochim. Acta*, 2007, **71**, 1197–1213.
25 C. Y. Lin, A. V. Turchyn, Z. Steiner, P. Bots, G. I. Lampronti and N. J. Tosca, *Geochim. Cosmochim. Acta*, 2018, **237**, 184–204.
26 X. Zhou, D. Liu, H. Bu, L. Deng, H. Liu, P. Yuan, P. Du and H. Song, *Solid Earth Sci.*, 2018, **3**, 16–29.
27 P. Mirjafari, K. Asghari and N. Mahinpey, *Ind. Eng. Chem. Res.*, 2007, **46**, 921–926.
28 J. J. De Yoreo and P. G. Vekilov, *Rev. Mineral. Geochem.*, 2003, **54**, 57–93.
29 J. Wu and R. J. Zeng, *Crystal Growth & Design*, 2017, **17**, 1854–1862.
30 D. Gebauer, A. Völkel and H. Cölfen, *Science*, 2008, **322**, 1819–1822.
31 J. D. Rodriguez-Blanco, S. Shaw, P. Bots, T. Roncal-Herrero and L. G. Benning, *J. Alloys Compd.*, 2012, **536**, S477–S479.
32 C. Kim, *J. Chem. Educ.*, 2003, **80**, 1351–1352.
33 P. Fadia, S. Tyagi, S. Bhagat, A. Nair, P. Panchal, H. Dave, S. Dang and S. Singh, *3 Biotech*, 2021, **11**, 457.
34 C. Ercole, P. Bozzelli, F. Altieri, P. Cacchio and M. Del Gallo, *Microsc. Microanal.*, 2012, **18**, 829–839.
35 X. Yin, F. Weitzel, C. Jiménez-López, E. Griesshaber, L. Fernández-Díaz, A. Rodríguez-Navarro, A. Ziegler and W. W. Schmahl, *Crystal Growth & Design*, 2020, **20**, 1467–1484.
36 T. Kawaguchi and A. W. Decho, *J. Cryst. Growth*, 2002, **240**, 230–235.
37 D. N. Azulay, R. Abbasi, I. Ben Simhon Ktorza, S. Remennik, A. Reddy M and L. Chai, *Crystal Growth & Design*, 2018, **18**, 5582–5591.
38 Y. Zhao, Z. Han, H. Yan, H. Zhao, M. E. Tucker, X. Gao, N. Guo, R. Meng and D. C. Owusu, *Front. Microbiol.*, 2021, **12**, 696557.
39 F. Shiraishi, T. Omori, N. Tomioka, S. Motai, H. Suga and Y. Takahashi, *Geochim. Cosmochim. Acta*, 2020, **285**, 55–69.
40 W. Guo, H. Ma, F. Li, Z. Jin, J. Li, F. Ma and C. Wang, *Geomicrobiol. J.*, 2013, **30**, 749–757.
41 C. Zhang, F. Li and J. Lv, *J. Cryst. Growth*, 2017, **478**, 96–101.